Electronic Supplementary Material (ESI) for Molecular BioSystems.

Supplementary information:

Section 1: Analysis of urine and serum samples

1.1 Urine and serum sample preparation

Biological fluid sample preparation protocol was conducted based on the modified method published by Beckonert *et al* [1]. Both urine and serum samples were thawed on ice. Of each urine sample, 200 µl of urine sample was brought up to 600 µl by addition of D_2O buffered with 0.24 M sodium phosphate (pH 7.4) containing sodium-3-trimethylsilyl-2,2,3,3,-d_4 propionate (TMSP) as an internal standard. 150µl of serum was brought up to 600 µl by addition of D_2O saline solution. The mixtures were centrifuged at 12,000 *g* at 4 °C for 5 min, and 580 µl of the supernatant were transferred to NMR tube for analysis.

1.2 NMR spectra acquisition.

NMR spectra were acquired using an Avance 600 spectrometer (Bruker Biospin) operating at 600.22 mHz and equipped with a 5-mm TXI cyroprobe at 300 K. The metabolomic analyses were performed as described previously[2] with minor modifications. The ^{1}H NMR spectra from urine and serum metabolites were acquired using a 1D NOESY-presat and Carr-Purcell-Meiboom-Gill sequence, respectively. A total of 128 transients were converted into 32,000 data points in a 12-min total acquisition time. The spectra phasing, and baseline correction were conducted using TOPSPIN (Version 2.1). Prior to data analysis, the raw NMR data were zero-filled to 64,000 data points with 0.3-Hz exponential line broadening prior to Fourier transformation.

1.3 Chemometric analysis

Prior to the multivariable analysis, the collected NMR spectra were segmented into chemical shift bins between 0.2 and 10.0 ppm, corresponding to the bin width of 0.005 ppm, by using custom-developed *ProMetab* software (version 3.3) [3] in MATLAB (The

Mathwork, Natick, MA). Spectral bins containing water and internal standard resonances were removed to prevent interference in subsequent multivariable analyses. To conduct comparisons between spectra, the integrated spectral area of the remaining bins was normalized to the creatinine and total integrated area for the urine and serum sample, respectively. The acquired data sets were log-transformed and Pareto-scaled prior to the multivariable analysis (principal component analysis; PCA) and partial least squares discriminant analysis (PLS-DA)) within Simca 13 (Umetrics, Umea, Sweden) to examine the clustering of the control and the naphthalene treatment groups.

1.4 Metabolite identification and statistical analysis

The metabolites responsible for the clustering within the pattern recognition models were identified by examining the corresponding loading plot. Metabolite peaks profiled from ^{1}H NMR spectra were referenced to literatures[4, 5], Chenomx software (Chenomx NMR Suite, version 6.1, Chenomx Inc., Canada), and the human metabolome database (HMDB)[6]. The chemical shifts of the mercapuric acids (*N*-acetylcysteine conjugated naphthalene metabolites) were confirmed using the purified metabolites which kindly provided by Professor Alan R. Buckpitt from University of California at Davis.

Section 2: Supplementary figures

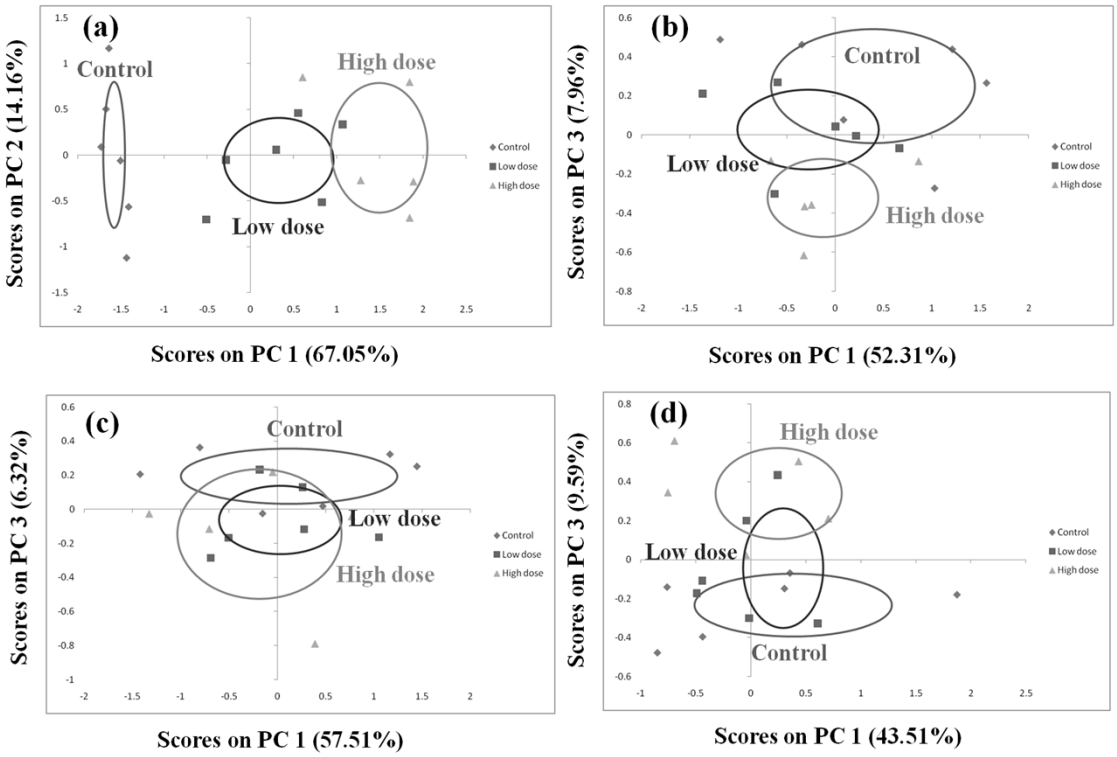

Figure S1. PCA score plots showing the clustering of the NMR spectra of mice urine collected at (a) 12, (b) 24, (c) 36, and (d) 48 h after different doses of naphthalene treatment; ● control (vehicle), ▩low dose (100 mg/kg body wt) and ▲high dose (200 mg/kg body wt). Ellipses represent mean ± SD of principal component scores for each group.

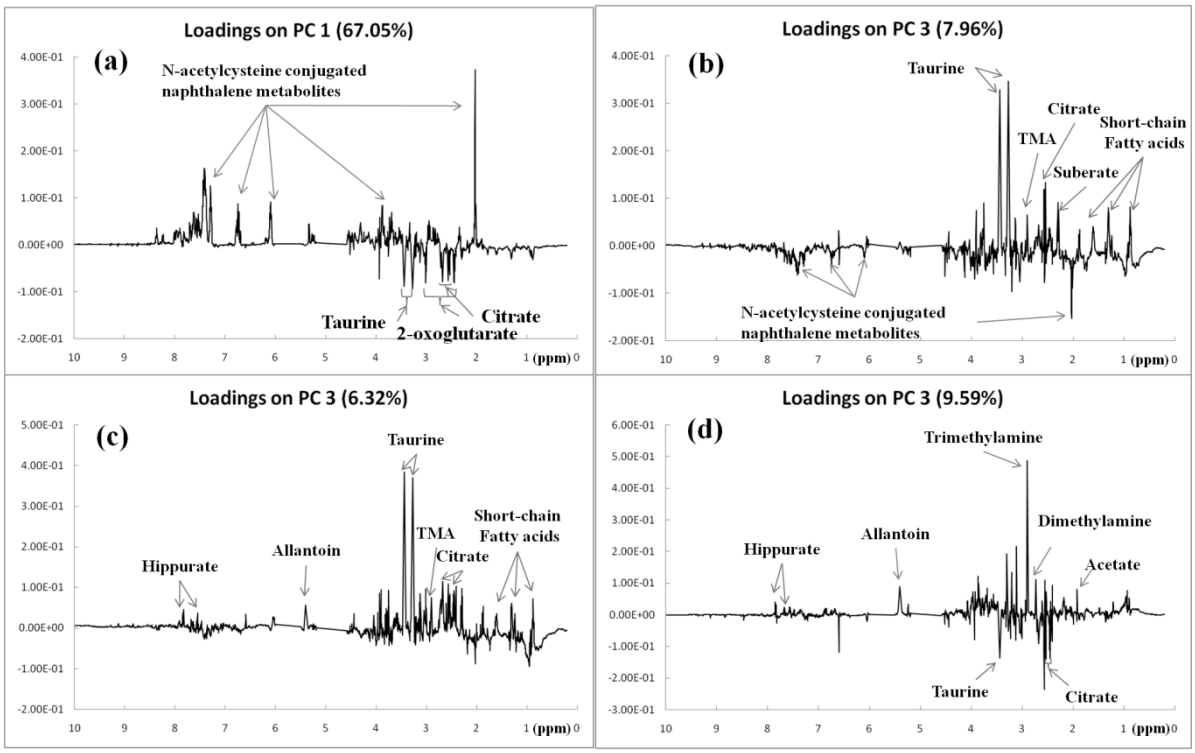

Figure S2. The corresponding PCA loadings plot from the NMR spectra of the mice urine collected at (a) 12h, (b) 24h, (c) 36h and (d) 48h after different doses of naphthalene treatment.

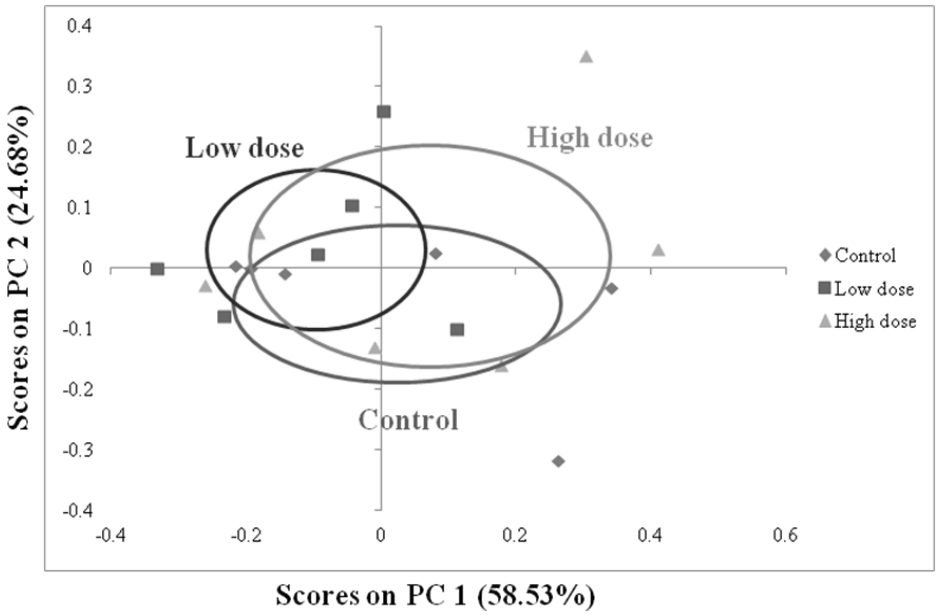

Figure S3. PCA score plots showing the clustering of the NMR spectra of mice serum collected at 48 h after different doses of naphthalene treatment; ● control (vehicle), ▓low dose (100 mg/kg body wt) and ▲high dose (200 mg/kg body wt). Ellipses represent mean ± SD of component scores for each group.

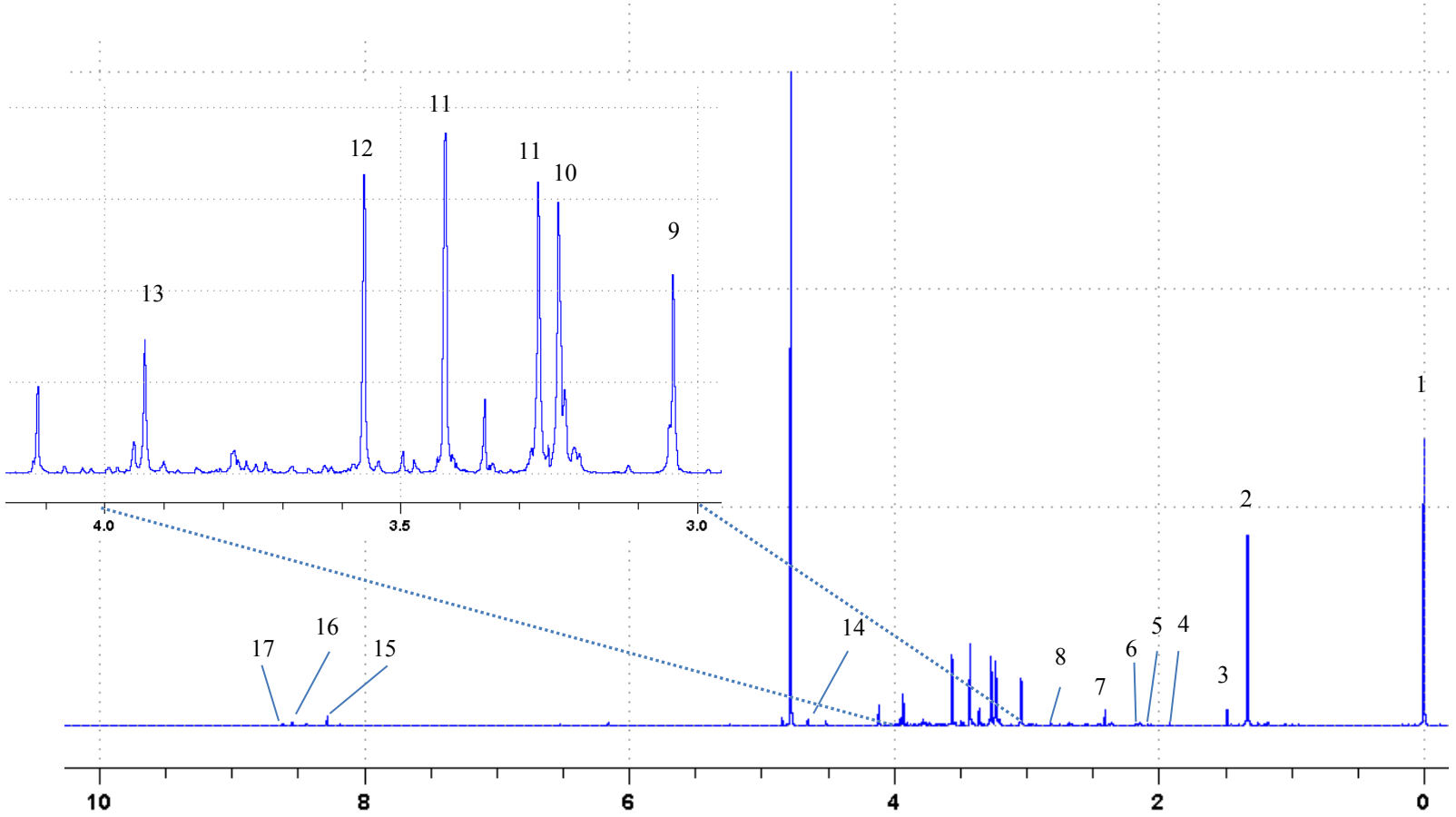

Figure S4 a. A typical J-resolved NMR spectrum of the hydrophilic extracts from lung tissue.

Key: 1: TMSP, 2: Lactate, 3: Alanine, 4: Acetate, 5: Glutamine, 6: Glutamate, 7: Succinate, 8: Aspartate, 9: Creatine, 10: Glycerophosphocholine, 11: Taurine, 12: Glycine, 13: Ascorbate, 14: Glucose, 15: NAD^+, 16: ADP, 17: AMP.

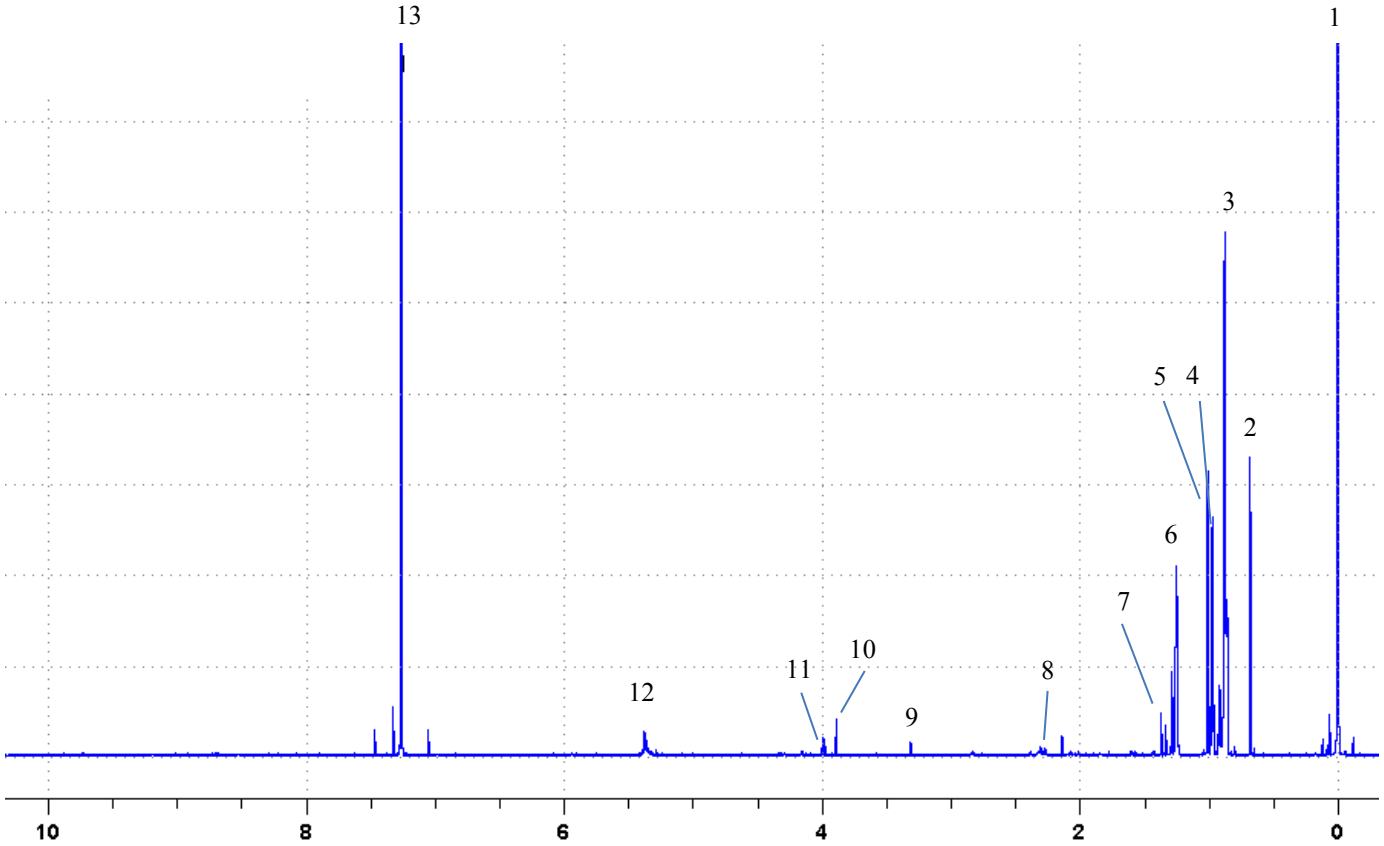

Figure S4 b A typical J-resolved NMR spectrum of the hydrophobic extracts from lung tissue

Key: 1: TMS, 2: Total cholesterol C-18 $\mathbf{H}_3$, 3: Total cholesterol C-26 $\mathbf{H}_3$/C-27 $\mathbf{H}_3$, 4: Fatty acyl chain $C\mathbf{H}_3(CH_2)_n$, 5: Total cholesterol C-21 $\mathbf{H}_3$, 6: CH_3 attached to C10 ($C19\mathbf{H}_3$)in free cholesterol, 7: Fatty acyl chain $(C\mathbf{H}_2)_n$, 8: Fatty acyl chain $-C\mathbf{H}_2CO$, 9: $N(C\mathbf{H}_3)_3$ of phosphorylcholine containing lipids, 10: Glycerol backbone C-1 $\mathbf{H}_2$, 11: Glycerol backbone C-3 $\mathbf{H}_2$, 12: Fatty acyl chain –**H**C=C**H**–,13: D-chloroform

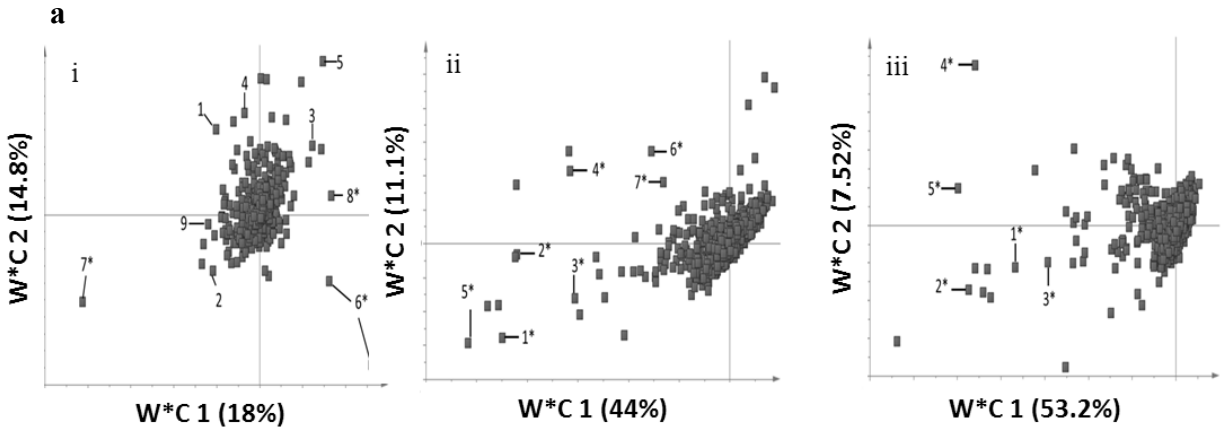

Figure S5 a. Loading plots showing the metabolites responsible for the separation in PLS-DA score plot of the lung extract. The loading plot for the score plot of the hydrophilic extracts after high dose naphthalene treatment (**i**), hydrophobic extracts after high dose (**ii**) and low dose (**iii**) naphthalene treatments
*indicates the metabolite changes were statistically significant.

Key in i: 1. Ascrobate, 2. AMP, 3.Creatine, 4.Glutamte, 5. Glycine, 6.Lactate, 7.Phosphocholine, 8.Succinate, 9 Taurine

Key in ii & iii: 1. C**H**$_3$ attached to C13(C18H$_3$) in cholesterol, 2. C**H**$_3$ attached to C26/C27 in cholesterol, 3. C**H**$_3$ attached to C21(C20H$_3$) in cholesterol, 4. C**H**$_3$ in fatty acyl chain 5. C**H**$_3$ attached to (CH$_2$)n fatty acyl chain (terminal), 6. C**H**$_3$ attached to C10(C19H$_3$) in cholesterol, 7. C**H**$_3$ attached to (C**H**$_2$)$_n$ fatty acyl chain (terminal)

b

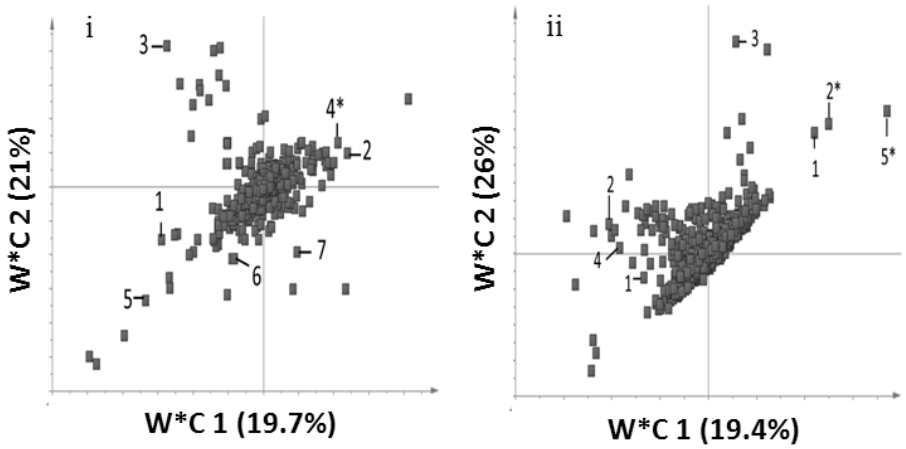

Figure S5 b. Loading plots showing the metabolites responsible for the separation in corresponding PLS-DA score plot of the liver extract. The loading plot for the score plot of the hydrophilic extracts after high dose naphthalene treatment (**i**), hydrophobic extracts after high dose (**ii**) naphthalene treatments

*indicates the metabolite changes were statistically significant.

Key in i 1. Alanine, 2.Ascrobate, 3.Glucose, 4.Glutamine, 5. Hypotaurine, 6.Lactate, 7.NAD^+

Key in ii 1.C**H**$_3$ attached to C13 (C18H$_3$) in cholesterol, 2. C**H**$_3$ attached to C10(C19H$_3$) in cholesterol, 3. C**H**$_3$ attached to C26/C27 in cholesterol, 4. -C1**H**$_2$- in glycerol backbone, 5. Phosphorylcholine-containing lipid.

c

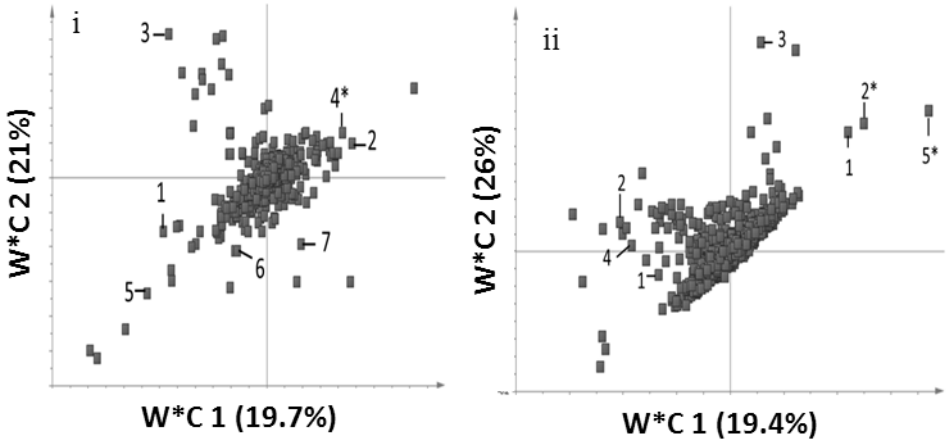

Figure S5 c. Loading plots showing the metabolites responsible for the separation in corresponding PLS-DA score plot of the kidney extract. The loading plot for the score plot of the hydrophilic extracts after high dose (**i**) and low dose (**ii**) naphthalene treatments.

*indicates the metabolite changes were statistically significant.

Key in i: 1. Choline, 2.Creatine, 3.Glutamate, 4.Glutamine, 5. Hypotaurine, 6.Succinate, 7.NAD^+

Key in ii: 1. Alanine, 2. Betaine, 3. Choline, 4.Creatine, 5. Cysteine, 6. Glutathione, 7. Hypotaurine

Section 3: Supplementary tables

Table S1: Significantly altered metabolites identified from the mice urine 12, 24, and 36 h after low (100mg/kg) or high (200mg/kg) dose naphthalene treatments using NMR.

Metabolite	Fold of changes [a]								
	K-W	12 h		K-W	24 h		K-W	36 h	
		L v C	L v C		L v C	L v C	-	L v C	L v C
2-oxoglutarate	●	0.74	0.62*	-	0.82	0.76	-	0.88	0.74
Citrate	●	0.73	0.52*	-	0.84	0.78	-	0.86	0.75
N-acetylcysteine conjugated naphthalene metabolites	●●●	3.18*	4.86*	●	1.01	1.28*	-	1.01	1.05
Taurine	●	0.81	0.70*	●	0.73*	0.64*	●	0.78*	0.75*

The changes of urinary metabolites 48 h after naphthalene treatment were insignificant. Therefore the data were excluded in the table.

[a] Fold changes of peak area relative to mean control. Values > 1 represent increase relative to the control group and value < 1 represent decrease relative to the control group.

LD, Low dose naphthalene treatment; HD, High dose naphthalene treatment.

●, p value <0.05 and ●●●, p value <0.001 determined by Kruskal-Wallis (K-W) test

* Indicates statistically significant metabolite changes relative to control by Mann-Whitney, p< 0.05.

Table S2 a. Hydrophilic metabolites identified from the mice lung using NMR after low (100mg/kg) or high (200mg/kg) dose naphthalene treatments.

Proton chemical shift (ppm)[a]	Metabolites	Kruskal-Wallis test (*p*- value)	Fold of changes [b]	
			L v C	L v C
1.91(s)^	Acetate	0.83	0.96	1.01
8.27(s)^,	ADP	0.89	0.97	0.98
1.50(d)^	Alanine	0.22	0.98	1.04
8.61(s)^, 9.33(s)	AMP	0.36	0.96	1.33
4.50(d) ^, 3.7(m)	Ascorbate	0.45	0.97	0.95
2.82(dd)^	Aspartate	0.27	0.9	0.87
3.02(s)^	Creatine	0.91	0.97	1.08
4.63(d), 5.23(m)^	Glucose	0.99	0.97	0.96
2.35(m)^, 2.01(m)	Glutamate	0.12	0.91	0.87
2.15(m), 2.46(m)^	Glutamine	0.16	0.99	1.13
3.56(s)^	Glycine	0.86	0.97	0.96
8.18(s)^, 8.42(s)	NAD^+	0.36	0.97	1
3.25(t), 3.41(t)^	Taurine	0.44	0.97	0.92
1.91(s)^	Acetate	0.94	0.96	1.01

[a] Peaks observed as singlet (s), doublet (d), double doublet (dd), triplet (t), quartet(q), pentet (p), and multiplet (m)

^The peaks selected for integrations

[b] Fold changes of peak area relative to mean control. Values > 1 represent increase relative to the control and values < 1 represent decrease relative to the control.

Table S2 b. Hydrophobic metabolites identified from the mice lung using NMR after low (100mg/kg) or high (200mg/kg) dose naphthalene treatments.

Proton chemical shift (ppm) [a]	Metabolites	Kruskal-Wallis test (*p*- value)	Fold of changes [b]	
			L v C	L v C
2.32(m)^	-C**H**$_2$CO- in fatty acyl chain	0.38	0.88	0.69
3.31(s)^	-N$^+$(CH)$_3$of phosphorylcholine containing lipids	0.41	0.89	0.94
4.15(m)^	C1**H**$_2$- in glycerol backbone	0.38	0.94	0.77
4.29(m)^	-C3**H**$_2$- in glycerol backbone	0.52	0.94	0.79
5.30-5.41(m)^	–**H**C=C**H**– in fatty acyl chain	0.26	0.91	0.81

[a] Peaks observed as singlet (s), doublet (d), double doublet (dd), triplet (t), quartet(q), pentet (p), and multiplet (m)

^The peaks selected for integrations

[b] Fold changes of peak area relative to mean control. Values > 1 represent increase relative to the control and values < 1 represent decrease relative to the control.

Table S3 a. Hydrophilic metabolites identified from the mice liver using NMR after low (100mg/kg) or high (200mg/kg) dose naphthalene treatments.

Proton chemical shift (ppm)[a]	Metabolites	Kruskal-Wallis test (*p*-value)	Fold of changes [b]	
			L v C	L v C
1.90(s)^	Acetate	0.61	1.1	1.07
1.47(d)^	Alanine	0.24	1.19	1.11
8.42(s)^, 9.33(s)	AMP	0.85	1.03	1.04
4.51(q)^	Ascorbate	0.41	1.13	1.27
2.82(dd)^	Aspartate	0.54	1.16	1.48
3.02(s)^	Creatine	0.7	0.97	1.08
4.63(d) ^, 5.22(d)	Glucose	0.64	0.96	0.89
2.56(m) ^, 3.77(t)	Glutathione	0.15	1.18	1.21
2.64(t)^, 3.34(t)	Hypotaurine	0.15	0.45	0.26
1.32(d) ^, 4.10(q)	Lactate	0.31	1.1	1.43
0.94(d)^	Leucine	0.99	1.01	0.99
8.26(s) ^, 8.60(s)	NAD+	0.78	1.09	1.13
2.39(s)^	Succinate	0.17	0.96	1.29
3.25(t), 3.41(t)^	Taurine	0.83	0.99	0.97
3.14(s)^	Unassigned	0.36	1.2	1.2
3.34(s)	Unassigned	0.94	0.97	0.94
0.98(d), 1.03(d)^	Valine	0.42	0.79	0.74

[a] Peaks observed as singlet (s), doublet (d), double doublet (dd), triplet (t), quartet(q), pentet (p), and multiplet (m)

^The peaks selected for integrations

[b] Fold changes of peak area relative to mean control. Values > 1 represent increase relative to the control and values < 1 represent decrease relative to the control.

Table S3 b. Hydrophobic metabolites identified from the extracted liver tissue using NMR after low (100mg/kg) or high (200mg/kg) dose naphthalene treatments

Proton chemical shift (ppm) [a]	Metabolites	Kruskal-Wallis test (*p*- value)	Fold of changes [b]	
			L v C	L v C
0.68(s)^	C**H**$_3$ attached to C13(C18H$_3$) in cholesterol	0.12	1.28	1.12
0.89(t)^	C**H**$_3$ attached to (CH$_2$)n fatty acyl chain (terminal)	0.53	1.18	1.01
1.01(s)^	C**H**$_3$ attached to C10(C19H$_3$) in cholesterol	0.08	1.39	1.16
1.28(m)^	C**H**$_3$ in fatty acyl chain (C4 and beyond saturated)	0.89	1.11	1.05
1.71(m)^	Multiple cholesterol protons	0.42	1.05	0.96
2.04(m)^	Allylic-CH=CH-C**H**$_2$	0.62	0.88	1.1
2.32(m)^	Fatty acyl chain -C**H**$_2$CO	0.72	0.82	0.7
2.38(m)^	RCH$_2$CH$_2$CO-	0.81	0.93	0.88
4.15(m)^	-C1**H**$_2$- in glycerol backbone	0.73	0.84	0.78
4.22(m)^	-C**H**$_2$-O-CO-R diacyl glycerol	0.84	0.88	0.84
4.29(m)^	-C3**H**$_2$- in glycerol backbone	0.75	0.82	0.78
5.26(m)^	-C2**H**$_2$- in glycerol backbone	0.26	0.82	0.91
5.29-5.43(m)^	Fatty acyl chain –HC=CH–	0.93	0.96	0.92

[a] Peaks observed as singlet (s), doublet (d), double doublet (dd), triplet (t), quartet(q), pentet (p), and multiplet (m)

^The peaks selected for peak-area comparison

[b] Fold changes of peak area relative to mean control. Values > 1 represent increase relative to the control group and value < 1 represent decrease relative to the control group.

Table S4. Hydrophilic metabolites identified from the mice kidney using NMR after low (100mg/kg) or high (200mg/kg) dose naphthalene treatments

Proton chemical shift (ppm) [a]	Metabolites	Kruskal-Wallis test (*p*-value)	Fold of changes [b]	
			L v C	L v C
8.27(s)^,	ADP	0.89	0.97	0.98
1.48(d)^	Alanine	0.56	1.15	1.2
8.40(s)^, 9.33(s)	AMP	0.29	0.96	0.97
2.80(dd)^	Aspartate	0.63	0.97	0.89
3.29(s), 3.89(s)^	Betaine	0.76	1.03	1.09
3.04(s)^	Creatine	0.96	0.95	1.04
3.36(dd)^	Cystine	0.35	1.13	1.2
4.65(d), 5.24(d)^	Glucose	0.11	1.33	1.02
2.34(m)^	Glutamate	0.69	0.94	0.9
2.64(t)^, 3.34(t)	Hypotaurine	0.35	0.45	0.26
1.32(d)^, 4.10(q)	Lactate	0.73	1.09	1.01
3.50(dd), 4.067(t)^	Myo-inositol	0.92	0.98	0.99
8.18(s)^, 8.42(s)	NAD+	0.35	0.97	1
2.39(s)^	Succinate	0.22	1.01	1.12
3.24(t), 3.42(t)^	Taurine	0.63	1.07	0.99
3.57(m)^	Unassigned	0.86	1.07	1.02

[a] Peaks observed as singlet (s), doublet (d), double doublet (dd), triplet (t), quartet(q), pentet (p), and multiplet (m)

^The peaks selected for peak-area comparison

[b] Fold changes of peak area relative to mean control. Values > 1 represent increase relative to the control group and value < 1 represent decrease relative to the control group.

Section 4: Phosphatidylcholine and ceramide species structural identification.

Throughout the analysis, variable importance projection (VIP) was conducted to estimate the importance of each variable in the projection used in the selected PLS-DA model, and the score threshold was set to 1.5, where the variables beyond this threshold would be selected for further analysis.

Protonated PC species had a common and significant fragment of *m/z* 184, which corresponded to the phosphocholine head group. Using this unique fragment, we were able to screen the PCs from the lipid extracts using precursor ion scan. However, this method was insufficient to discriminate the many diverse PCs. To perform such discriminations, we adopted several mass spectrum interpretations proposed earlier[7, 8], which enabled the differentiation of esterified acyl, alkyl ether (*O*-alkyl-) or vinyl ether (*O*-alk-1-enyl-) fatty acids chain *via* an adducting sodium ion (Figure S7). Briefly, diacyl-PC (e.g PC (16:0/18:1)), the $[M+Na-183]^+$ ion ($[M+Na-HPO_4(CH_2)_2N(CH_3)_3]^+$) was dominant (~90%) but was complemented with the minor (<40%) $[M+Na-205]^+$ ion ($[M+Na-NaPO_4(CH_2)_2N(CH_3)_3]^+$) in the product ion spectrum (Figure S7 a). In contrast to diacyl-PC, the product ion spectra of the sodium-adducted alkylacyl-PC and alk-1-enylacyl-PC revealed that the both relative ion intensities for $[M+Na-183]^+$ and $[M+Na-205]^+$ appeared to be minor (Figure S7b & c). The product ion scan of sodiated alk-1-enylacyl-PC (e.g P-18:0/18:1) showed that it possessed a greater ion intensity of $[M+Na-183]^+$ than $[M+Na-205]^+$ (Supplementary Figure 2c), and *vice versa* for the sodiated alkylacyl-PC (e.g O-16:0/16:0) (Supplementary Figure 2b). Moreover, it was remarkable that the ion intensities for both $[M+Na-183]^+$ and $[M+Na-205]^+$ for sodiated alkylacyl-PC were consistently less than 50% of the base ion (Figure S7b & c).

Once the PC subclass was determined, the ion spectrum of demethylation $[M-Me]^-$ was generated to illustrate the fatty acid substituents within PCs (Supplementary Figure S8). The loss of one methyl moiety from the choline head group of PCs can generate useful product ions, which assisted us in determining the carbon number and degree of unsaturation that existed within fatty acid substituents of PCs. For example PC (16:0/18:1) product ions at *m/z* 281 and 255, corresponding to the 18:1 and 16:0-carboxylate anions during deductive interference, were observed for PC (16:0/18:1). The least liable of the *sn-2* acyl groups (*m/z* 281), which is prone to be lost as a complete chain [9], led to its intensity being approximately 3-fold higher than that of *sn-1* (*m/z* 255), which may suggest PC structure assignment (Figure S8a). Furthermore, the presentation of one carboxylate anion signal suggested that the symmetrical diacyl-PC produced the same

carboxylate anion from both the *sn-1* and *sn-2* positions (Figure S8b & c) and previously, Han and Gross 1995 proposed the cleavage of the ether (from alkylacyl-PC) or vinyl ether linkage (from alk-1-enylacyl-PC) did not happen easily.

a

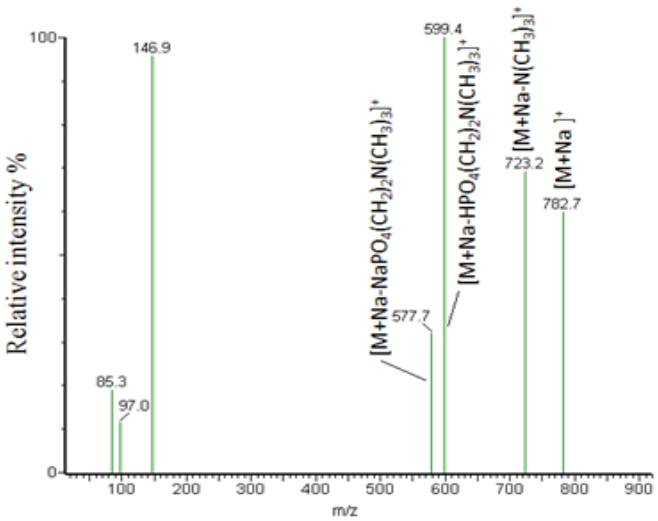

b

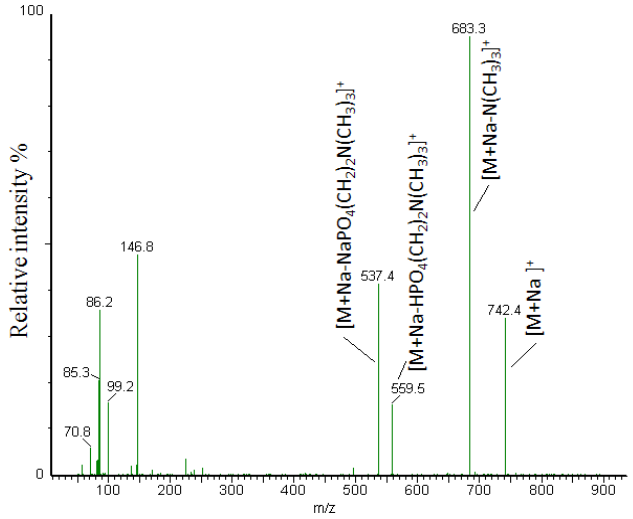

c

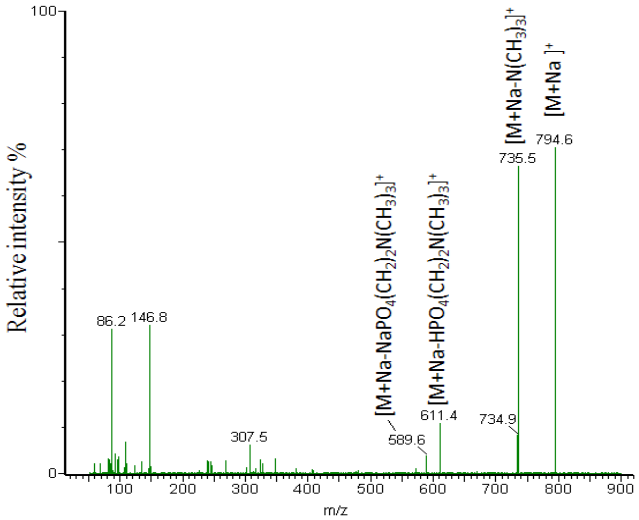

Figure S7. Collision-induced fragment tendam mass spectra of sodiated $[M+Na]^+$ **(a)** PC(16:0/18:1), **(b)** PC(O-16:0/16:0) and **(c)** PC(P-18:0/18:1). The selected PC molecular ions were collided with argon (0.1 mL/min) using a collision energy of 28 eV by the rf-only quadrupole.

a

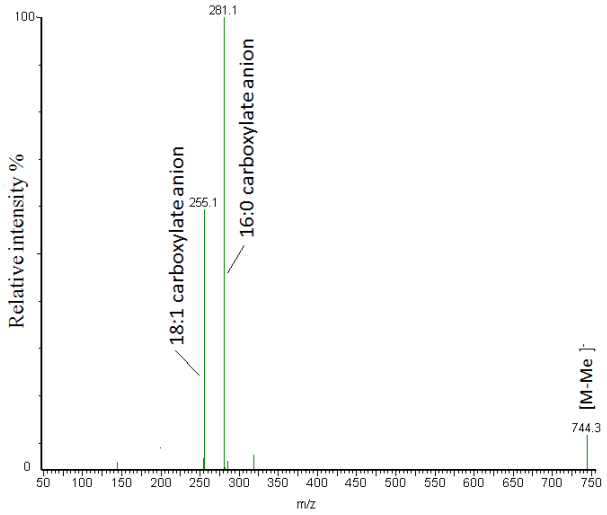

b

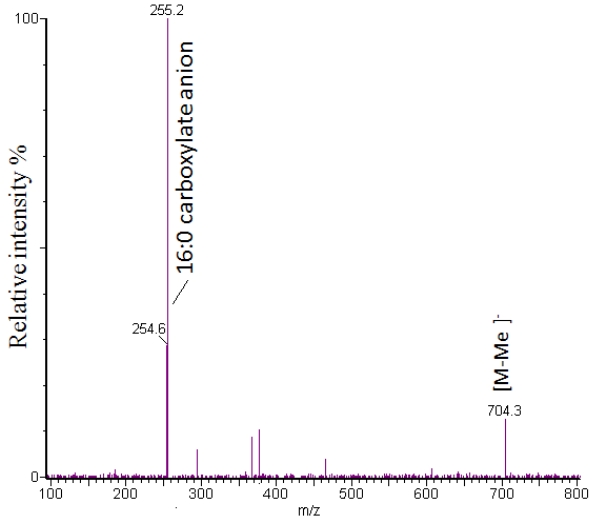

c

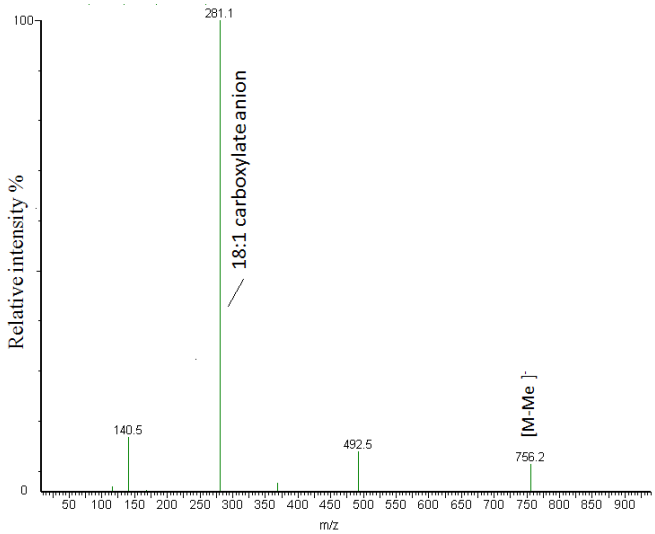

Figure S8. Collision-induced fragment tendam mass spectra of demethylated $[M\text{-}Me]^-$ **(a)** PC(16:0/18:1), **(b)** PC(O-16:0/16:0) and **(c)** PC(P-18:0/18:1). The selected PC molecular ions were collided with argon (0.1 mL/min) using a collision energy of 30 eV by the rf-only quadrupole.

Protonated ceramides and C1P produce a common fragment of *m/z* 264, which corresponded to the sphingosine backbone (d18:1). Through precursor ion scanning, the difference between ceramide and ceramide-1-phosphate could not be distinguished. Therefore, we performed a product ion scan $[M+H]^+$ to differentiate the phosphorylated ceramides from other ceramides. Figure S9 a illustrates the loss of $[M+H-98]^+$ ions, corresponding to the loss of phosphoric acid (H_3PO_4) on the phosphorylated ceramides. None of the phosphoric acid fragments could be observed (Figure S9 b) in ceramide. The complete description of the fatty acid substituents could be archived by performing the mass balance for the detected *m/z* values [7]

a

b

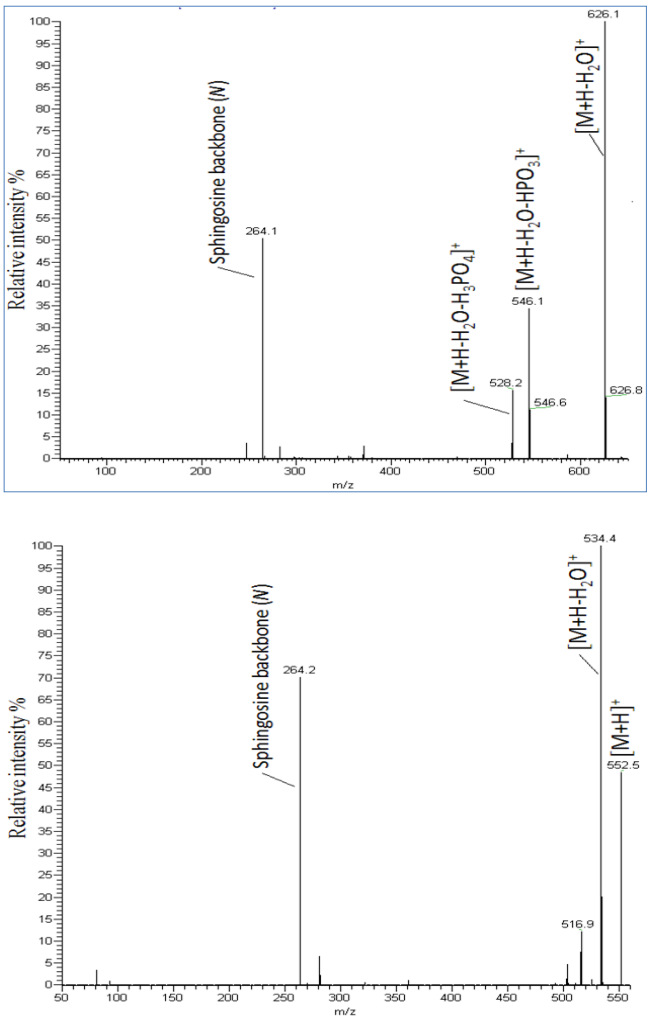

Figure S9. Collision-induced fragment tendam mass spectra of protonated $[M+H]^+$ **(a)** C1P (d18:1/18:0) and **(b)** Ceramide (d18:1/17:0). The selected ceramide molecular ions were collided with argon (0.1 mL/min) using a collision energy of 25 eV by the rf-only quadrupole

References

1. O. Beckonert, H. C. Keun, T. M. D. Ebbels, J. Bundy, E. Holmes, J. C. Lindon and J. K. Nicholson, Metabolic profiling, metabolomic and metabonomic procedures for NMR spectroscopy of urine, plasma, serum and tissue extracts, *Nat. Protocols*, 2007, **2**, 2692-2703.
2. C. F. B. Kim, E. L. Jackson, A. E. Woolfenden, S. Lawrence, I. Babar, S. Vogel, D. Crowley, R. T. Bronson and T. Jacks, Identification of Bronchioalveolar Stem Cells in Normal Lung and Lung Cancer, *Cell*, 2005, **121**, 823-835.
3. M. Viant, Environmental Metabolomics Using ^{1}H-NMR Spectroscopy in *Environmental Genomics*, ed. C. C. Martin, Humana Press, 2008, vol. 410, pp. 137-150.
4. M. Oostendorp, U. F. H. Engelke, M. A. A. P. Willemsen and R. A. Wevers, Diagnosing inborn errors of lipid metabolism with proton nuclear magnetic resonance spectroscopy, *Clin. Chem.*, 2006, **52**, 1395-1405.
5. J. K. Nicholson, P. J. D. Foxall, M. Spraul, R. D. Farrant and J. C. Lindon, 750 MHz ^{1}H and ^{1}H-^{13}C NMR spectroscopy of human blood plasma, *Anal. Chem.*, 1995, **67**, 793-811.
6. D. S. Wishart, C. Knox, A. C. Guo, R. Eisner, N. Young, B. Gautam, D. D. Hau, N. Psychogios, E. Dong, S. Bouatra, R. Mandal, I. Sinelnikov, J. Xia, L. Jia, J. A. Cruz, E. Lim, C. A. Sobsey, S. Shrivastava, P. Huang, P. Liu, L. Fang, J. Peng, R. Fradette, D. Cheng, D. Tzur, M. Clements, A. Lewis, A. De Souza, A. Zuniga, M. Dawe, Y. Xiong, D. Clive, R. Greiner, A. Nazyrova, R. Shaykhutdinov, L. Li, H. J. Vogel and I. Forsythe, HMDB: a knowledgebase for the human metabolome, *Nucleic Acids Res.*, 2009, **37**, D603-D610.
7. Y. S. Ling, H. J. Liang, M. H. Lin, C. H. Tang, K. Y. Wu, M. L. Kuo and C. Y. Lin, Two-dimensional LC-MS/MS to enhance ceramide and phosphatidylcholine species profiling in mouse liver, *Biomed. Chromatogr.*, 2014, **In press** DOI 10.1002/bmc.3162.
8. C. H. Tang, P. N. Tsao, C. Y. Chen, M. S. Shiao, W. H. Wang and C. Y. Lin, Glycerophosphocholine molecular species profiling in the biological tissue using UPLC/MS/MS, *J. Chromatogr. B*, 2011, **879**, 2095-2106.
9. X. Han and R. W. Gross, Structural determination of picomole amounts of phospholipids via electrospray ionization tandem mass spectrometry, *Journal of the American Society for Mass Spectrometry*, 1995, **6**, 1202-1210.